



CHORUS

This is the accepted manuscript made available via CHORUS. The article has been published as:

Photoemission and dynamical mean field theory study of electronic correlations in a t_{2g}^5 metal SrRhO_3 thin film

Yujun Zhang, Minjae Kim, Jernej Mravlje, Changhee Sohn, Yongseong Choi, Joerg Stempfer, Yasushi Hotta, Akira Yasui, John Nichols, Ho Nyung Lee, and Hiroki Wadati

Phys. Rev. B **101**, 085134 — Published 24 February 2020

DOI: [10.1103/PhysRevB.101.085134](https://doi.org/10.1103/PhysRevB.101.085134)

Photoemission and Dynamical Mean Field Theory Study of Electronic Correlation in a t_{2g}^5 Metal of SrRhO₃ Thin Film

Yujun Zhang,^{1,2,3,*} Minjae Kim,^{4,5,†} Jernej Mravlje,⁶ Changhee Sohn,⁷ Yongseong Choi,⁸ Joerg Strempler,⁸ Yasushi Hotta,⁹ Akira Yasui,¹⁰ John Nichols,¹¹ Ho Nyung Lee,⁷ and Hiroki Wadati^{2,3}

¹*Institute of High Energy Physics, Chinese Academy of Science, Yuquan Road 19B, Shijingshan District, Beijing, 100049, China*

²*Graduate School of Materials Science, University of Hyogo, 3-2-1 Kouto, Kamigori-cho, Ako-gun, Hyogo 678-1297, Japan*

³*Institute for Solid State Physics, University of Tokyo, 5-1-5 Kashiwanoha, Chiba 277-8581, Japan*

⁴*Department of Physics and Astronomy, Rutgers University, Piscataway, New Jersey 08854, USA*

⁵*Collège de France, 11 place Marcelin Berthelot, 75005 Paris, France*

⁶*Jožef Stefan Institute, Jamova 39, Ljubljana, Slovenia*

⁷*Materials Science and Technology Division, Oak Ridge National Laboratory, Oak Ridge, Tennessee 37831, USA*

⁸*Advanced Photon Source, Argonne National Laboratory, Argonne, Illinois 60439, USA*

⁹*Department of Engineering, University of Hyogo, 2167 Shosha, Himeji, Hyogo 671-2280, Japan*

¹⁰*Japan Synchrotron Radiation Research Institute (JASRI), 1-1-1 Kouto, Sayo, Hyogo 679-5198, Japan*

¹¹*Department of Physics and Astronomy, University of Arkansas at Little Rock, Little Rock, AR, 72204, USA*

Perovskite rhodates are characterized by intermediate strengths of both electronic correlation as well as spin-orbit coupling (SOC) and usually behave as moderately correlated metals. A recent publication (Phys. Rev. B 95, 245121(2017)) on epitaxial SrRhO₃ thin films unexpectedly reported a bad-metallic behavior and suggested the occurrence of antiferromagnetism below 100 K. We studied this SrRhO₃ thin film by hard x-ray photoemission spectroscopy and found a very small density of states (DOS) at the Fermi level (E_F), which is consistent with the **previously** reported bad-metallic behavior. However, **the absence of DOS** persists up to room temperature, which contradicts with the explanation of antiferromagnetic transition at ~ 100 K. We also employed electronic structure calculations within the framework of density functional theory and dynamical mean-field theory. In contrast to the experimental results, our calculations indicate metallic behavior of both bulk SrRhO₃ and the SrRhO₃ thin film. The thin film exhibits stronger correlation effects than the bulk, but is still far from an insulating state in our calculations. The calculated uniform magnetic susceptibility is substantially larger in the thin film than that in the bulk. We also investigated the role of SOC and found only a moderate modulation of the band structure. Hence SOC is not expected to significantly affect the electronic correlation in SrRhO₃. Extrinsic effects of **finite-thickness effects beyond our calculations** and film imperfections may play an important role to induce the negligible spectral weight at E_F .

INTRODUCTION

$4d$ transition metal compounds are characterized by the moderate strengths of both electronic correlation and spin-orbit coupling (SOC) compared to their strongly correlated $3d$ and strongly spin-orbit-coupled $5d$ counterparts. Nevertheless, $4d$ systems do exhibit interesting physical properties as well. Notable examples are found especially in the perovskite ruthenate family: unconventional superconductivity in Sr₂RuO₄ [1, 2], ferromagnetism (FM) in SrRuO₃ [3], and current-induced insulator-metal transition in Ca₂RuO₄ [4, 5], etc. Magnetism plays an important role in many $4d$ systems. Spin-triplet superconductivity in Sr₂RuO₄ was argued to be related to ferromagnetic spin fluctuations [1, 2]. FM is realized in SrRuO₃ [3, 6] while CaRuO₃ [6, 7] and Sr₃Ru₂O₇ [8, 9] are presumably close to FM. On the other hand, Ca₂RuO₄ is a special case that exhibits an antiferromagnetic (AFM) insulating ground state and insulator-metal transition [10, 11]. However, magnetic ordering is rarely observed in other perovskite $4d$ oxides except radioactive SrTcO₃ [12–14].

Since Rh is the neighbor of Ru in the $4d$ transition metal series, Rh-based perovskite oxides, such as SrRhO₃ [15–18], Sr₂RhO₄ [19–23] and Sr₃Rh₂O₇ [24], have also attracted considerable research attention. In the bulk state, these rhodates are usually correlated metals without magnetic ordering. Among them, SrRhO₃ has the most simple crystal structure. As first reported by Yamaura *et al.* [15], bulk SrRhO₃ has a GdFeO₃-type distorted perovskite structure with space group $Pnma$. Metallic transport behavior was observed down to 1.8 K [15] and covalent doping of Ca at the Sr-site does not have significant influence on the metallic state of SrRhO₃ [16]. Nevertheless, there are several reports that strongly indicate the instability towards magnetic ordering in SrRhO₃. An enhanced paramagnetic susceptibility [15] and related theoretical investigations [17] suggest that SrRhO₃ is near a quantum critical point with significant ferromagnetic quantum fluctuation.

Recently, epitaxial SrRhO₃ thin films were successfully synthesized and their transport and magnetic properties were reported by Nichols *et al.* [18]. No FM was observed in the SrRhO₃ thin films but subtle anomalies

appeared at around 100 K in magnetization and magnetoresistance, which indicates the possibility of a magnetic transition. **The resistivity of SrRhO₃ is very weakly dependent on temperature at high temperature and exhibits an upturn upon cooling below 100 K, showing a weakly insulating behavior.** Based on the density functional theory (DFT) $+U$ calculations, Ref. [18] suggested that a C-type AFM structure is energetically favorable, **but there is no direct experimental confirmation so far.**

In the present work, we studied SrRhO₃ epitaxial thin film by hard x-ray photoemission spectra (HAXPES) to characterize its electronic structure and the correlation effects, as was earlier done for other perovskite transition metal oxides [13, 25–27]. Instead of a coherent peak, a negligible density of states (DOS) near Fermi level (E_F) was observed. This is the case for **both room temperature and 80 K**, which is not compatible with the interpretation of the resistivity upturn upon cooling **at ~ 100 K** in terms of the gap opening induced by AFM order. Realistic dynamic mean field theory (DMFT) calculations were conducted to investigate the electronic correlation and instability towards magnetic ordering in SrRhO₃. These calculations yield a Mott insulating state only for interaction parameters well above any plausible value for SrRhO₃ and no magnetic ordering was found as well. On the other hand, the calculated magnetic susceptibility of the SrRhO₃ thin film is much larger than **the one in the bulk**, indicating a stronger instability towards magnetic ordering in the thin film. Since SOC can also play a significant role in $4d$ perovskite oxides such as Sr₂RuO₄ [20, 28] and Sr₂RhO₄ [20–22], we investigated the band structure of SrRhO₃ by also taking SOC into account. Given that the changes of the band structure are modest, we judge that SOC cannot drive a Mott insulating state in SrRhO₃ thin film. **The discrepancy between our experiment and calculation could be attributed to either the simplifications in our calculations such as not taking into account the finite-thickness effects and the presence of the substrate, or the extrinsic effects on the experimental side such as localization effects due to the film imperfections.**

METHODS

A 9 nm-thick (around 23 unit cells) epitaxial SrRhO₃ thin film was grown on a SrTiO₃(001) single crystalline substrate by pulsed laser deposition. The details of the fabrication methods and basic characterizations of the sample were previously reported in Ref. [18].

HAXPES of the SrRhO₃ thin film was measured at BL47XU of SPring-8. The incidence angle of **horizontally** linearly polarized 7.94 keV hard x-ray was set at 1° and photoemission spectra were collected by a Scienta R-4000 electron energy analyzer with an energy resolution of around 250 meV. Soft x-ray photoemission spec-

tra (SXPES) were measured by a PHI 5000 VersaProbe system (ULVAC-PHI Inc.) with perpendicular incidence of Al $K\alpha$ radiation (1468.7 eV). The energy resolution of the SXPES measurement was around 450 meV. The position of E_F and the energy resolution of both photoemission measurements were determined by measuring and fitting the spectra of a Au reference sample, which was in electrical contact with the SrRhO₃ thin film. For temperature dependent HAXPES measurement, a He-flow cryostat was employed to cool the sample down to 80 K.

X-ray linear dichroism (XLD) and resonant magnetic x-ray diffraction (RMXD) measurements of the SrRhO₃ thin film at the Rh L edge were carried out at beamline 4-ID-D of Advanced Photon Source. For the room temperature XLD measurement, linearly polarized x-rays with electric field component E perpendicular and parallel to the sample surface were utilized to measure the x-ray absorption spectra (XAS). The incidence angle of the x-rays was set at around 3° and the XAS signal was collected by partial fluorescence yield mode. RXMD measurement was conducted at 30 K by cooling the sample with an ARS He Displex cryocooler.

For the DFT calculation, we used the Wien2k package [29] and local density approximation (LDA) was employed for the calculation of the exchange correlation potential. **For crystal structure of the SrRhO₃ thin film, we used the in-plane symmetry and lattice constants of the SrTiO₃ substrate ($a=b=3.905$ Å, $c=4.043$ Å) as reported in Ref. [18]. The internal positions of atoms are relaxed in the unit cell by using DFT. Space group of $Amm2$ was used and polar distortion was allowed. The relaxation of positions of atoms gives rise to changes of atomic position less than 0.01 Å for polar distortions. The rotation of octahedra was not considered due to the absence of orthorhombicity reported by Ref. [18]. Thus, the SrRhO₃ thin film is described as a bulk structure imposed by the epitaxial strain of the reported thin film. Neither the finite thickness of the thin film nor the presence of the substrate were explicitly taken into account. For the DFT+DMFT calculation, we used the TRIQS framework [30–33]. We considered e_g , t_{2g} , and oxygen $2p$ orbitals of SrRhO₃ and treated t_{2g} orbitals dynamically by using a rotationally invariant Kanamori Hamiltonian with parameters $U = 2.3$ eV and $J = 0.4$ eV, which has been used to precisely describe the neighboring ruthenates [6, 34]. The U value presented here is in the Kanamori interaction Hamiltonian. **Our calculations are “one-shot” but we checked that the charge self-consistency does not lead to a more correlated behavior.** To compute the magnetic susceptibility by DFT+DMFT, we applied a magnetic field of 5 meV (around 86 T) and calculated the corresponding spin polarization.**

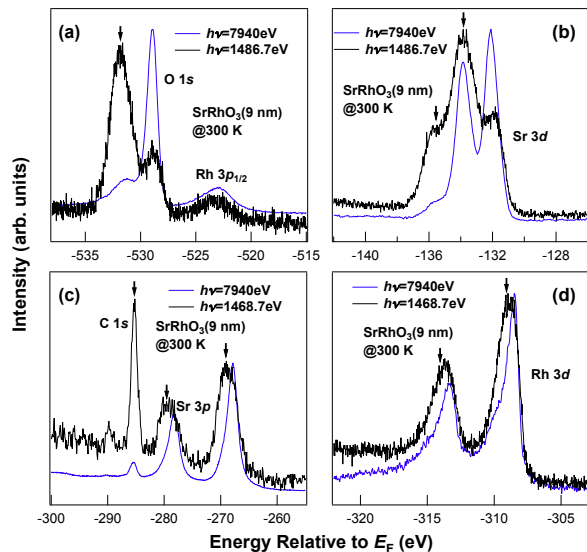


FIG. 1. Room temperature (a) O $1s$ and Rh $3p_{1/2}$; (b) Sr $3d$; (c) C $1s$ and Sr $3p$; (d) Rh $3d$ core level photoemission spectra of the SrRhO₃ thin film. Photon energies of 7940 eV and 1486.7 eV are used for HAXPES and SXPES measurements, respectively. The arrows indicate the surface components, which are enhanced in SXPES.

PHOTOEMISSION RESULTS

Fig.1 shows the core level HAXPES and SXPES results of the SrRhO₃ thin film. HAXPES is quite bulk-sensitive and the detection depth is beyond the thickness of the film since the photoemission signal of Ti in the substrate can be observed. On the other hand, SXPES is very surface sensitive, whose typical detection depth is around 1 to 2 nm [35]. It can be noticed in Fig.1 that surface components (-532 eV O $1s$ peak in Fig.1(a); -135.7 eV/-133.9 eV Sr $3d$ peaks in Fig.1(b); C $1s$ contamination signal at -285.5 eV in Fig.1(c); left shoulders of Sr $3p$ in Fig.1(c) and left shoulders of Rh $3d$ in Fig.1(d)) have different binding energies compared to the bulk components (-528.9 eV O $1s$ peak in Fig.1(a); -133.9 eV/-132.1 eV Sr $3d$ peaks in Fig.1(b); main peaks of Sr $3p$ at -278.2 eV/-267.9 eV in Fig.1(c) and main peaks of Rh $3d$ at -313.3 eV/-308.5 eV in Fig.1(d)). The surface components have little influence on the HAXPES results. The binding energies of peaks in the Rh $3d$ spectra are also consistent with previous reports of Rh⁴⁺ oxides [36].

The valence band HAXPES and SXPES results are displayed in Fig.2(a). Due to the different photoionization cross-sections of p and d levels for hard and soft x-rays [37], HAXPES is more sensitive to p levels and SXPES is more sensitive to d levels. By comparing the HAXPES and SXPES results, it can be concluded that the features in the energy range from -10 eV to -3 eV are dominated by O $2p$ emission and the features above -3 eV mainly come from Rh $4d$ emission. Fig.2(b) shows

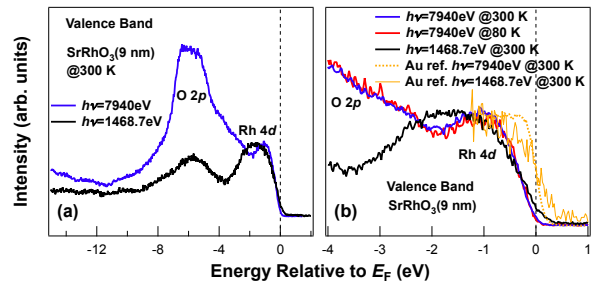


FIG. 2. (a) Room temperature valence band photoemission spectra of the SrRhO₃ thin film. (b) Enlarged valence band photoemission spectra of the SrRhO₃ thin film. The data of reference Au are also shown. Photon energies of 7940 eV and 1486.7 eV are used for HAXPES and SXPES measurements, respectively.

the valence band spectra in an expanded region near E_F . Surprisingly, the coherent peak is totally absent for both HAXPES and SXPES. A very small DOS near E_F starts to increase substantially only below -0.2 eV. The difference between HAXPES and SXPES at E_F is mainly due to the different energy resolution of HAXPES and SXPES. By comparing with the corresponding spectra of the Au reference sample, it is clear that both HAXPES and SXPES have very small intensity at E_F , although we cannot predicate that a gap is fully opened. It should be noted that the SrTiO₃ substrate could also contribute to the HAXPES valence band spectra due to the large detection depth of HAXPES. However, since SrTiO₃ is an insulator with d^0 configuration, it has nearly no contribution to the intensity above -3 eV [38]. These results are certainly inconsistent with a good metal as the coherent peak is absent, but the gap is not clearly developed either. The observed photoemission results are not inconsistent with the overall behavior of resistivity reported in Ref. [18] that is almost temperature independent and hence neither clearly insulating nor clearly metallic.

In Ref. [18], the possibility of magnetic ordering in the SrRhO₃ thin film with a transition temperature of around 100 K was proposed. To investigate the temperature dependence of the electronic structure in the SrRhO₃ thin film, we also conducted HAXPES measurement at 80 K. However, nearly no temperature dependence was observed, as shown in Fig.2(b). Since the SrTiO₃ substrate has a structural phase transition near this temperature [39], the reported anomalies in transport properties [18] may be related to the change of substrate strain rather than a real magnetic transition.

DFT AND DFT+DMFT RESULTS

The photoemission results above suggest negligibly small DOS near E_F in the SrRhO₃ thin film, in contrast

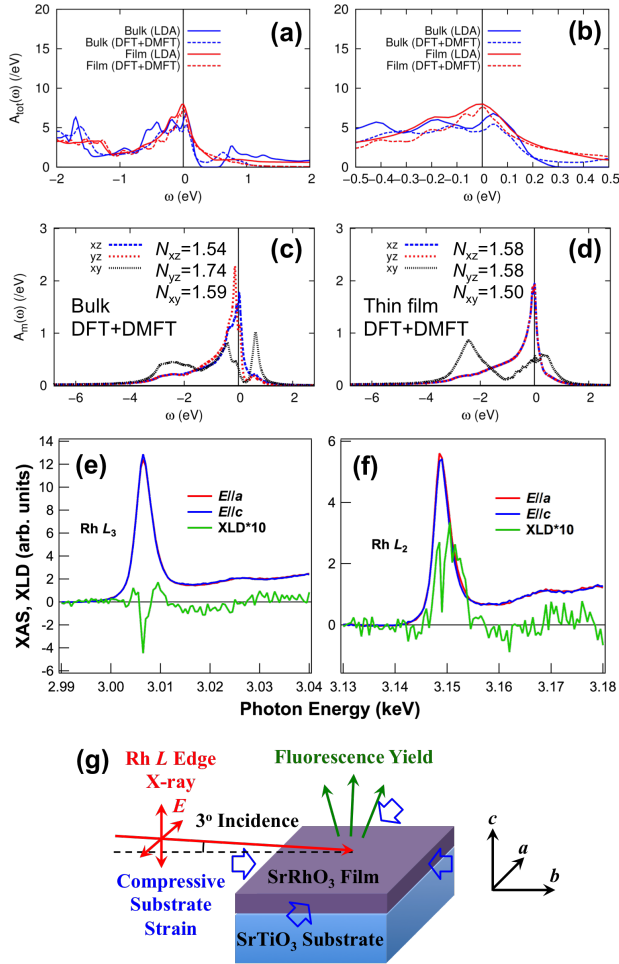


FIG. 3. Total DOS $A_{\text{tot}}(\omega)$ calculated by DFT and DFT+DMFT (without SOC, $T=58$ K) for the bulk and the thin film in (a) wider energy range and (b) narrower energy range. Orbital-resolved DFT+DMFT (without SOC) DOS $A_m(\omega)$ at $T=58$ K for (c) the bulk and (d) the thin film. N in the figures indicates the orbital occupation. ω is the energy relative to E_F . (e,f) Rh L edge XAS and XLD spectra of the SrRhO₃ thin film. (g) Schematic of the XLD measurement for the SrRhO₃ thin film under compressive substrate strain.

to bulk SrRhO₃ that exhibits metallic behavior [15]. Because of the possible role of electronic correlation in this distinction, we turn to the DFT(+DMFT) calculations performed for both the bulk and the thin film as follows.

The total DOS obtained by DFT+DMFT is shown in Fig.3(a,b). One can notice that DFT+DMFT calculations predict metallic behavior for both the bulk and the thin film. Only moderate effects of electronic correlation with renormalization of $Z \approx 0.5$ are observed ($Z = (1 - \frac{\partial \text{Re}\Sigma(\omega)}{\partial \omega})^{-1}|_{\omega \rightarrow 0}$), as obtained by the self-energy results shown in Fig.4. The thin film is slightly more correlated with smaller Z , but no major difference between the thin film and the bulk is observed, in contrast to the experimental results. We found that the critical interaction

parameter U_c (with fixed Hund's coupling of $J=0.4$ eV) is above 10 eV for the bulk structure of SrRhO₃, as shown in the appendix. This U_c of metal-insulator transition is consistent with Ref. [40] considering the given bandwidth (W) of ~ 4 eV in DFT calculation for both the bulk and the thin film structures of SrRhO₃. With N -fold degenerate band, the strong coupling approach for Mott transition drives the critical parameter of the Mott transition as $U_c - 3J = \sqrt{NW}$ [41]. From the Brinkman-Rice approach to Mott transition, the critical parameter of the Mott transition is given by $U_c - 3J = NW$ [42]. The critical parameter of Mott transition, $U_c - 3J$, of SrRhO₃ is within a reasonable range between $\sqrt{3}W$ and $3W$, with consideration of the threefold degenerate t_{2g} orbitals.

According to the orbitally resolved DFT+DMFT DOS in Fig.3(c,d), the occupancy of the xy orbital (1.50) is smaller than that of the xz/yz orbitals (1.58) in the thin film, which is consistent with the Rh L_2 edge XLD results. As depicted in Fig.3(e-g), XLD is defined as the difference of XAS measured by using incident x-rays with $E//a$ and $E//c$, where a and c are the in-plane [100] and the out-of-plane [001] directions, respectively. Since the XAS intensity at the Rh L edge is proportional to the number of $4d$ holes, a positive XLD signal indicates a preferred occupation of out-of-plane $4d$ orbitals and less occupation of in-plane $4d$ orbitals. Note that the sign change in the L_3 edge XLD spectrum could often be observed in other systems as well, while the spectrum at the L_2 edge can usually reflect the orbital occupation more unambiguously [43]. These experimental and computational results are consistent with the biaxial compressive strain from the SrTiO₃ substrate [18].

On the other hand, in contrast to the strong orbital anisotropy of spectral weight between the xy and the xz/yz orbitals, the orbital dependence of quasiparticle renormalization is not as strong as that in Sr₂RuO₄ [34, 44], which is consistent with the claim in Ref. [45] that correlation effects are weaker in SrRhO₃ than in perovskite ruthenates. The electronic correlation changes the center energy of the xz , yz , and xy orbitals. In the DFT calculation, the center energy of the xy orbital is 618 meV higher than that of the xz/yz orbitals in the SrRhO₃ thin film. In the DFT+DMFT self-energy of the thin film (Fig.4(b)), the xz/yz orbitals are shifted up with respect to the xy level for 212 meV, as shown by the difference of the real part of self-energy at zero energy. The peak position of the Van-hove singularity in thin film structure is 0.003 eV in DFT. While in the DFT+DMFT calculations, the peak position of Van-hove singularity is 0.007 eV for thin film structure, encountering correlation-induced quasiparticle renormalization of $Z \sim 0.5$. As a result, the effective energy level of xy with respect to that of xz/yz is reduced from 618 meV to 404 meV by electronic correlation in DFT+DMFT calculations. The net effect of this redistribution of energy

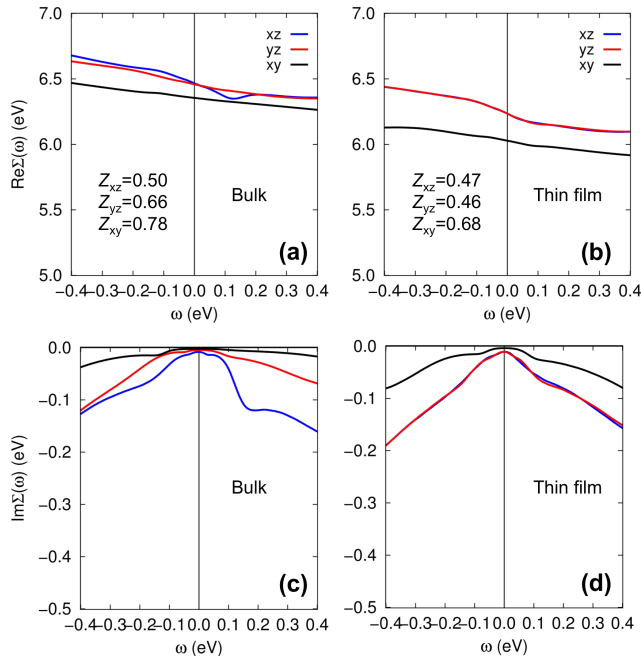


FIG. 4. DFT+DMFT (without SOC) self-energy for the bulk and the thin film at $T=58$ K. (a) Real part, bulk; (b) Real part, thin film; (c) Imaginary part, bulk; (d) Imaginary part, thin film. Corresponding renormalization factors Z are listed in the figures.

levels is that the value of the DOS at E_F is reduced by correlation, as shown in Fig.5(a). Reduction of the DOS in the bulk structure is consistent with the small electronic component of the experimental specific heat [15]. It is noteworthy that the xz/yz orbitals have a larger DOS at E_F than the xy orbital in the thin film. Meanwhile, the result that $Z \approx 0.5$ for all orbitals implies that electronic correlation is not so sensitive to the value of the DOS at small energies, which is different from Hund's metals such as ruthenates and iron-based superconductors [34, 40].

We also calculated the uniform magnetic susceptibility of both the bulk and the thin film, as shown in Fig.5(b). In contrast to the self-energy, the calculated magnetic susceptibility does show a substantially different behavior in the thin film. The magnetic susceptibility of the thin film is 6 to 7 times larger and exhibits a stronger temperature dependence than that of the bulk case, in contrast to the nearly temperature independent total DOS in the bulk and the thin film (Fig.5(a)). The difference in the calculated magnetic susceptibility for the bulk and the thin film can be understood as follows. First, the larger total DOS at E_F in the thin film with respect to that in the bulk (Fig.3(b)) gives rise to a larger magnetic susceptibility. Second, the stronger electronic correlation of the xz/yz orbitals in the thin film compared to that in the bulk (Fig.4(a-d)) give rise to a larger magnetic insta-

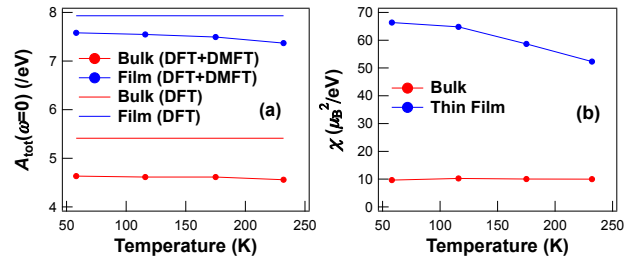


FIG. 5. (a) Temperature dependent total DFT+DMFT (without SOC) DOS at E_F for the bulk and the thin film. The total DOS calculated by DFT for the bulk and the thin film are also plotted for comparison. (b) Temperature dependent magnetic susceptibility calculated by DFT+DMFT (without SOC) for the bulk and the thin film.

bility in the thin film. Third, the sharper slope in the DOS of the xz/yz orbitals in the thin film compared to that in the bulk (Fig.3(c,d)) gives rise to a stronger temperature dependence of the magnetic susceptibility in the thin film. These results are inherited from the tetragonal symmetry of the lattice of the thin film, which gives rise to the presence of the Van-hove singularity of the xz/yz orbitals near E_F .

In our photoemission results, it is clearly shown that there is a negligible temperature dependence of the DOS between 80 K and 300 K. The present DFT+DMFT results with similar renormalization for both the bulk and the thin film suggest that if there is a real transition of the electronic structure, it will not be a simple metal-insulator transition with a Mott gap, because the critical U for the Mott transition is larger than 10 eV, which is well above any reasonable value of $U \lesssim 3$ eV for a $4d$ element [23, 46]. The larger magnetic susceptibility in the thin film compared to that in the bulk implies that the SrRhO₃ thin film has a much stronger intrinsic instability towards magnetically ordered phases. This magnetic instability is mainly induced by the anisotropy of the crystal environment, such as crystal field symmetry and bandwidth anisotropy. However, whether this larger magnetic susceptibility is a side effect (or indicator) of some actual electronic instability that in turn is responsible for the experimentally observed negligible DOS at E_F is an open question.

Earlier DFT calculations suggested the occurrence of an AFM state in SrRhO₃ thin films [18]. We investigated the possibility of magnetic ordering by DFT+ U calculation and found that we need $U > 5$ eV for the stabilization of the C-type AFM state, which is likely a too large value for the $4d$ shell [46–48]. We also conducted RXMD experiments at the Rh L edges to attest the existence of AFM ordering peaks. Due to the restricted Q range that the Rh L edge x-ray (around 3 keV) can reach, Q vectors of (0 0 0.5) (A-type), (0.5 0.5 1) (C-type) and (0.5 0.5 0.5) (G-type) were investigated at 30 K but

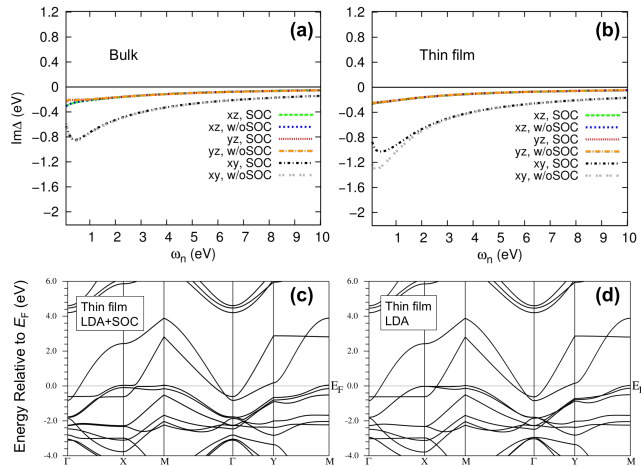


FIG. 6. Hybridization functions in the initial step of DFT+DMFT calculation for (a) the bulk and (b) the thin film. ω_n is the Matsubara frequency. Band structures for the thin film calculated by DFT (c) with and (d) without SOC.

no observable diffraction appeared within the detection limit.

DISCUSSION OF NEGLIGIBLE DOS AT E_F IN SrRhO_3 THIN FILM

In principle, a possible origin of the small **experimental** DOS at E_F and the absence of a coherent peak could be SOC, which can play an important role in t_{2g}^5 iridates [49, 50]. If SOC were strong enough to split the $J_{\text{eff}}=1/2$ and $J_{\text{eff}}=3/2$ states significantly, one could expect that an insulating behavior would be promoted by the half-filled $J_{\text{eff}}=1/2$ band. We are unable to run the DFT+DMFT calculation in the presence of SOC because of the fermionic sign problem in the hybridization expansion quantum Monte Carlo impurity solver that we use [23, 32, 33]. An interaction expansion solver could be used to alleviate this problem, which remains a task for the future [51]. To get an impression of the possible role of SOC nevertheless, we calculated the hybridization functions, which determine the behavior of the DMFT calculation in the presence of SOC. The results shown in Fig.6(a,b) imply that SOC moderately affects the electronic structure of SrRhO_3 . As also shown by DFT results with and without SOC in Fig.6(c,d), in the thin film, due to the SOC-induced band splitting around E_F (along Γ to X line), SOC reduces the hybridization function of the xy orbital **at small energies <2 eV** (Fig.6(b)). Provided the fact that quasiparticle residue $Z \approx 0.5$ and a small orbital dependence of the Fermi velocity, we suggest that SOC can not trigger the metal-insulator transition but might give rise to a strong magnetic instability in the SrRhO_3 thin film. For bulk SrRhO_3 , the effect of

SOC is even smaller due to the lower lattice symmetry, as shown in Fig.6(a). Note that even in SrIrO_3 , the $5d$ counterpart of SrRhO_3 , SOC is still not strong enough to trigger an insulating behavior [50]. Moreover, we can get similar conclusion by analyzing the branching ratio (BR) of XAS results shown in Fig.3(e,f). The BR between the white-line intensities of Rh L_3 and L_2 edges is related to the ground-state expectation value of the angular part of SOC [52]. A large deviation from the statistical BR=2 indicates the presence of strong SOC effects. The experimental BR at the Rh $L_{3,2}$ edges is close to the statistical value of 2 (estimated as ~ 2.3 from Fig.3(e,f)), indicating weak SOC effects in the SrRhO_3 thin film. This is in contrast to the Ir $5d$ cases where large deviations (BR > 4) from the statistical value, thus large SOC, have been observed [53–55]. The consistency of orbital polarization in the XLD and the DFT+DMFT results for SrRhO_3 thin film supports that SOC does not have sizable effects on the electronic correlation. The SOC would not have much effect on quasiparticle renormalization factors Z , but only specific k points with degeneracy of t_{2g} orbitals would be affected by SOC [28].

There is also the possibility of more complicated magnetic or charge ordering with incommensurate propagation wave vectors, such as helical magnetic ordering or spin/charge density waves, which could be responsible for the absence of coherent peak in the SrRhO_3 thin film. The weakness of possible diffraction peaks can also be the reason to hinder their detection. Thus, we think that the possibility of orderings still cannot be completely ruled out in SrRhO_3 thin film. Another possible mechanism could be the formation of polarons induced by electron-phonon interaction. However, change of electronic structure induced by either orderings or polaron should be highly temperature dependent [56], which is **inconsistent with our observation** of temperature-independent experimental valence band structure.

Considering such discrepancy between experiment and calculation, **namely** that we found negligible DOS at E_F in experiment while obtaining a metallic state with critical U above 10 eV in calculation, it is also necessary to discuss **other** extrinsic effects. **One possible factor to cause the discrepancy is that in our calculation, the finite thickness of SrRhO_3 thin film and the presence of SrTiO_3 are not taken into account, which can cause significant modification of electronic structure.** For instance, SrVO_3 thin film becomes insulating in DMFT calculation due to surface crystal field splitting [57]. Lattice mismatch and coupling at the interface between the film and the substrate can also influence the rotation of oxygen octahedra and induce insulating behavior in DMFT calculations [58]. With full consideration of the finite thickness and the existence of substrate, the DMFT results could possibly differ a lot from present results. **On the other hand,** Anderson localization induced by sample imperfections and defects can lead to similar negligible DOS

near E_F in systems such as Na doped WO_3 [56] and Fe doped TaS_2 [59]. It is worth noticing that the negligible DOS at E_F in some of these systems has close connection with polaron formation and shows strong temperature dependence of the photoemission spectral shape [56], while in some other systems, the localization effects show less temperature dependence [59]. It is mentioned that there is a critical thickness of around 15 nm to obtain SrRhO_3 thin film with pure perovskite phase on SrTiO_3 [18]. Consequently, it is reasonable to infer that the SrRhO_3 film we are investigating is in a thermodynamically metastable state and the negligible DOS at E_F is likely induced by relatively temperature-independent localization effects originating from bulk defects and non-stoichiometry, as well as imperfections at the surface or interface of the thin film.

CONCLUSIONS

In summary, we experimentally and theoretically investigated the effects of electronic correlation in SrRhO_3 . The photoemission results indicate a negligible DOS at E_F in the SrRhO_3 thin film with little temperature dependence. We considered SrRhO_3 within band-structure calculation taking into account the electronic correlation with a DFT+DMFT approach. In our calculation the small DOS at E_F could not be reproduced, rather a moderately correlated metallic behavior was observed. Our attempts to detect the AFM magnetic diffraction by experiment and to stabilize magnetically ordered states in the calculations both failed. But the calculation did reveal an interesting behavior in the magnetic susceptibility that is substantially larger for the thin film. This result is mainly induced by the difference of crystal anisotropy between the bulk and the thin film structures. Extrinsic factors like **finite thickness effects and defect-induced Anderson localization** may be the explanation of the discrepancy between our experiments and calculations. Further experimental and theoretical investigations are warranted to clarify the situation, including investigation of the role of crystal imperfections, further investigations of the possible phase transitions in SrRhO_3 on the experimental side and taking explicit account of SOC as well as direct simulation of the thin film in a slab geometry on the theoretical side.

ACKNOWLEDGMENTS

This work was supported by Grant-in-Aid for JSPS fellows (No. 17F17327). The HAXPES experiments at SPring-8 were performed under the approval of the Japan Synchrotron Radiation Research Institute (Proposal No. 2018B1449). This research used resources of the Advanced Photon Source, a U.S. Department of En-

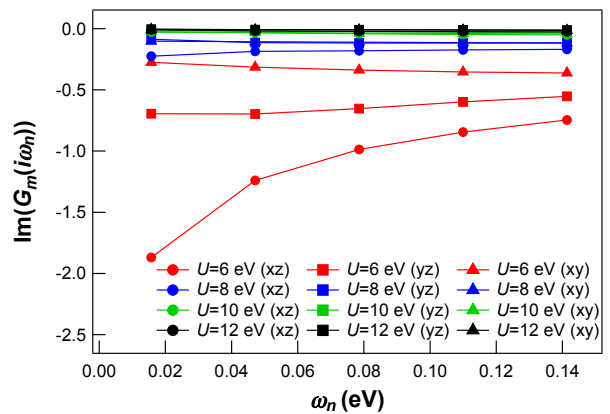


FIG. 7. Estimation of the critical interaction strength U_c of bulk SrRhO_3 . $\text{Im}(G_m(i\omega_n))$ is the imaginary part of orbital dependent local Green's function in the Matsubara axis.

ergy (DOE) Office of Science User Facility operated for the DOE Office of Science by Argonne National Laboratory under Contract No. DE-AC02-06CH11357. The work at ORNL was supported by the U.S. Department of Energy, Office of Science, Basic Energy Sciences, Materials Sciences and Engineering Division. M. K. acknowledges support from Grant No. NSF DMR-1733071, and grateful to CPHT computer support team. We are thankful to the support and advices provided by A. Georges, V. R. Cooper, S. F. Yuk, and A. Rastogi. And we also acknowledge the support provided by K. Ikeda, S. Sakuragi and H. Kinoshita, as well as enlightening discussion about this work with J. W. Kim and H. Zhou during our beamtime in Advanced Photon Source.

APPENDIX

The critical interaction strength U_c for the Mott transition can be identified by looking at the imaginary part of orbital dependent local Green's function in the Matsubara axis, $\text{Im}(G_m(i\omega_n))$, at different ω_n . The condition of $\text{Im}(G_m(i\omega_n)) \rightarrow 0$ when $\omega_n \rightarrow 0$ is the criterion for the metal-insulator transition [60]. In Fig. 7 we plot the $\text{Im}(G_m(i\omega_n))$ for different orbitals m and several values of U of bulk SrRhO_3 , keeping fixed $J = 0.4$ eV. Above $U = 8$ eV the values of $\text{Im}G_m(0)$ become small but remain finite for the xz orbital. For U above 10 eV the gap opens up completely with negligible $\text{Im}G_m(0)$ for all orbitals. This indicates that the U_c of SrRhO_3 is around 10 eV when keeping $J=0.4$ eV. Similar results with critical U above 10 eV are also observed for the thin film structure.

* zhangyujun@ihep.ac.cn

† garix.minjae.kim@gmail.com

- [1] Y. Maeno, H. Hashimoto, K. Yoshida, S. Nishizaki, T. Fujita, J. G. Bednorz, and F. Lichtenberg, Superconductivity in a layered perovskite without copper, *Nature* 372,532 (1994).
- [2] A. P. Mackenzie and Y. Maeno, The superconductivity of Sr_2RuO_4 and the physics of spin-triplet pairing, *Reviews of Modern Physics* 75,657 (2003).
- [3] A. Kanbayasi, Magnetic properties of SrRuO_3 single crystal, *Journal of the Physical Society of Japan* 41, 1876 (1976).
- [4] F. Nakamura, M. Sakaki, Y. Yamanaka, S. Tamaru, T. Suzuki, and Y. Maeno, Electric-field-induced metal maintained by current of the Mott insulator Ca_2RuO_4 , *Scientific Reports* 3, 2536 (2013).
- [5] C. Sow, S. Yonezawa, S. Kitamura, T. Oka, K. Kuroki, F. Nakamura, and Y. Maeno, Current-induced strong diamagnetism in the Mott insulator Ca_2RuO_4 , *Science* 358, 1084 (2017).
- [6] H. T. Dang, J. Mravlje, A. Georges, and A. J. Millis, Electronic correlations, magnetism, and Hund's rule coupling in the ruthenium perovskites SrRuO_3 and CaRuO_3 , *Physical Review B* 91, 195149 (2015).
- [7] G. Cao, S. McCall, M. Shepard, J. E. Crow, and R. P. Guertin, Thermal, magnetic, and transport properties of single-crystal $\text{Sr}_{1-x}\text{Ca}_x\text{RuO}_3$ ($0 \leq x \leq 1.0$), *Physical Review B* 56, 321 (1997).
- [8] G. Cao, S. McCall, and J. E. Crow, Observation of itinerant ferromagnetism in layered $\text{Sr}_3\text{Ru}_2\text{O}_7$ single crystals, *Physical Review B* 55, R672 (1997).
- [9] S. Ikeda, Y. Maeno, S. Nakatsuji, M. Kosaka, and Y. Uwatoko, Ground state in $\text{Sr}_3\text{Ru}_2\text{O}_7$: Fermi liquid close to a ferromagnetic instability, *Physical Review B* 62, R6089 (2000).
- [10] S. Nakatsuji, S. Ikeda, and Y. Maeno, Ca_2RuO_4 : New Mott insulators of layered ruthenate, *Journal of the Physical Society of Japan* 66, 1868 (1997).
- [11] J. P. Carlo, T. Goko, I. M. Gat-Malureanu, P. L. Russo, A. T. Savici, A. A. Aczel, G. J. MacDougall, J. A. Rodriguez, T. J. Williams, G. M. Luke, C. R. Wiebe, Y. Yoshida, S. Nakatsuji, Y. Maeno, T. Taniguchi, and Y. J. Uemura, New magnetic phase diagram of $(\text{Sr,Ca})_2\text{RuO}_4$, *Nature Materials* 11, 323 (2012).
- [12] D. Oka, Y. Hirose, S. Nakao, T. Fukumura, and T. Hasegawa, Intrinsic high electrical conductivity of stoichiometric SrNbO_3 epitaxial thin films, *Physical Review B* 92, 205102 (2015).
- [13] H. Wadati, J. Mravlje, K. Yoshimatsu, H. Kumigashira, M. Oshima, T. Sugiyama, E. Ikenaga, A. Fujimori, A. Georges, A. Radetnac, K. S. Takahashi, M. Kawasaki, and Y. Tokura, Photoemission and DMFT study of electronic correlations in SrMoO_3 : Effects of Hund's rule coupling and possible plasmonic sideband, *Physical Review B* 90, 205131 (2014).
- [14] E. E. Rodriguez, F. Poineau, A. Llobet, B. J. Kennedy, M. Avdeev, G. J. Thorogood, M. L. Carter, R. Seshadri, D. J. Singh, and A. K. Cheetham, High temperature magnetic ordering in the 4d perovskite SrTcO_3 , *Physical Review Letters* 106, 067201 (2011).
- [15] K. Yamaura and E. Takayama-Muromachi, Enhanced paramagnetism of the 4d itinerant electrons in the rhodium oxide perovskite SrRhO_3 , *Physical Review B* 64, 224424 (2001).
- [16] D. J. Singh, Prospects for quantum criticality in perovskite SrRhO_3 , *Physical Review B* 67, 054507 (2003).
- [17] K. Yamaura, Q. Huang, D. P. Young, M. Arai, and E. Takayama-Muromachi, Electronic properties of the novel 4d metallic oxide SrRhO_3 , *Physica B: Condensed Matter* 329, 820 (2003).
- [18] J. Nichols, S. F. Yuk, C. Sohn, H. Jeon, J. W. Freeland, V. R. Cooper, and H. N. Lee, Electronic and magnetic properties of epitaxial SrRhO_3 films, *Physical Review B* 95, 245121 (2017).
- [19] R. S. Perry, F. Baumberger, L. Balicas, N. Kikugawa, N. J. C. Ingle, A. Rost, J. F. Mercure, Y. Maeno, Z. X. Shen, and A. P. Mackenzie, Sr_2RhO_4 : a new, clean correlated electron metal, *New Journal of Physics* 8, 175 (2006).
- [20] M. W. Haverkort, I. S. Elfimov, L. H. Tjeng, G. A. Sawatzky, and A. Damascelli, Strong spin-orbit coupling effects on the Fermi surface of Sr_2RuO_4 and Sr_2RhO_4 , *Physical Review Letters* 101, 026406 (2008).
- [21] G. Q. Liu, V. N. Antonov, O. Jepsen, and O. K. Andersen, Coulomb-enhanced spin-orbit splitting: The missing piece in the Sr_2RhO_4 puzzle, *Physical Review Letters* 101, 026408 (2008).
- [22] C. Martins, M. Aichhorn, L. Vaugier, and S. Biermann, Reduced effective spin-orbital degeneracy and spin-orbital ordering in paramagnetic transition-metal oxides: Sr_2IrO_4 versus Sr_2RhO_4 , *Physical Review Letters* 107, 266404 (2011).
- [23] G. Zhang and E. Pavarini, Optical conductivity, Fermi surface, and spin-orbit coupling effects in Sr_2RhO_4 , *Physical Review B* 99, 125102 (2019).
- [24] K. Yamaura, Q. Huang, D. P. Young, Y. Noguchi, and E. Takayama-Muromachi, Crystal structure and electronic and magnetic properties of the bilayered rhodium oxide $\text{Sr}_3\text{Rh}_2\text{O}_7$, *Physical Review B* 66, 134431 (2002).
- [25] M. Takizawa, D. Toyota, H. Wadati, A. Chikamatsu, H. Kumigashira, A. Fujimori, M. Oshima, Z. Fang, M. Lippmaa, M. Kawasaki, and H. Koinuma, Manifestation of correlation effects in the photoemission spectra of $\text{Ca}_{1-x}\text{Sr}_x\text{RuO}_3$, *Physical Review B* 72, 060404 (2005).
- [26] A. Sekiyama, H. Fujiwara, S. Imada, S. Suga, H. Eisaki, S. I. Uchida, K. Takegahara, H. Harima, Y. Saitoh, I. A. Nekrasov, G. Keller, D. E. Kondakov, A. V. Kozhevnikov, T. Pruschke, K. Held, D. Vollhardt, and V. I. Anisimov, Mutual experimental and theoretical validation of bulk photoemission spectra of $\text{Sr}_{1-x}\text{Ca}_x\text{VO}_3$, *Physical Review Letters* 93, 156402 (2004).
- [27] M. Takizawa, M. Minohara, H. Kumigashira, D. Toyota, M. Oshima, H. Wadati, T. Yoshida, A. Fujimori, M. Lippmaa, M. Kawasaki, H. Koinuma, G. Sordi, and M. Rozenberg, Coherent and incoherent d band dispersions in SrVO_3 , *Physical Review B* 80, 235104 (2009).
- [28] M. Kim, J. Mravlje, M. Ferrero, O. Parcollet, and A. Georges, Spin-orbit coupling and electronic correlations in Sr_2RuO_4 , *Physical Review Letters* 120, 126401 (2018).
- [29] P. Blaha, K. Schwarz, G. K. H. Madsen, D. Kvasnicka, and J. Luitz, An augmented plane wave+ local orbitals program for calculating crystal properties, *Universität*

- Wien, Austria (2001).
- [30] M. Aichhorn, L. Pourovskii, P. Seth, V. Vildosola, M. Zingl, O. E. Peil, X. Deng, J. Mravlje, G. J. Kraberger, C. Martins, M. Ferrero, and O. Parcollet, TRIQS/DFTTools: a TRIQS application for *ab initio* calculations of correlated materials, *Computer Physics Communications* 204, 200 (2016).
- [31] O. Parcollet, M. Ferrero, T. Ayril, H. Hafermann, I. Krivenko, L. Messio, and P. Seth, TRIQS: A toolbox for research on interacting quantum systems, *Computer Physics Communications* 196, 398 (2015).
- [32] P. Seth, I. Krivenko, M. Ferrero, and O. Parcollet, TRIQS/CTHYB: A continuous-time quantum Monte Carlo hybridisation expansion solver for quantum impurity problems, *Computer Physics Communications* 200, 274 (2016).
- [33] E. Gull, A. J. Millis, A. I. Lichtenstein, A. N. Rubtsov, M. Troyer, and P. Werner, Continuous-time Monte Carlo methods for quantum impurity models, *Reviews of Modern Physics* 83, 349 (2011).
- [34] J. Mravlje, M. Aichhorn, T. Miyake, K. Haule, G. Kotliar, and A. Georges, Coherence-incoherence crossover and the mass-renormalization puzzles in Sr_2RuO_4 , *Physical Review Letters* 106, 096401 (2011).
- [35] M. P. Seah and W. A. Dench, Quantitative electron spectroscopy of surfaces: A standard data base for electron inelastic mean free paths in solids, *Surface and Interface Analysis* 1, 2 (1979).
- [36] T. K. Le, D. Flahaut, H. Martinez, N. Andreu, D. Gonbeau, E. Pachoud, D. Pelloquin, and A. Maignan, The electronic structure of the $\text{CuRh}_{1-x}\text{Mg}_x\text{O}_2$ thermoelectric materials: An x-ray photoelectron spectroscopy study, *Journal of Solid State Chemistry* 184, 2387 (2011).
- [37] M. B. Trzhaskovskaya, V. I. Nefedov and V. G. Yarzhevsky, Photoelectron angular distribution parameters for elements $Z=1$ to $Z=54$ in the photoelectron energy range 100–5000 eV, *Atomic Data and Nuclear Data Tables* 77, 97 (2001).
- [38] Y. Haruyama, S. Kodaira, Y. Aiura, H. Bando, Y. Nishihara, T. Maruyama, Y. Sakisaka, and H. Kato, Angle-resolved photoemission study of SrTiO_3 (100) and (110) surfaces, *Physical Review B* 53, 8032 (1996).
- [39] N. Ohama, H. Sakashita, and A. Okazaki, The temperature dependence of the lattice constant of SrTiO_3 around the 105 K transition, *Phase Transitions: A Multinational Journal* 4, 81 (1984).
- [40] A. Georges, L. de' Medici, and J. Mravlje, Strong correlations from Hunds coupling, *Annual Review of Condensed Matter Physics* 4, 137 (2013).
- [41] O. Gunnarsson, E. Koch, R. M. Martin, Mott-Hubbard transition in systems with large degeneracy: Application to doped fullerenes, *Physical Review B* 54, R11026 (1996).
- [42] J. P. Lu, Metal-insulator transitions in degenerate Hubbard models and A_xC_{60} , *Physical Review B* 49, 5687 (1994).
- [43] D. Pesquera, G. Herranz, A. Barla, E. Pellegrin, F. Bondino, E. Magnano, F. Sanchez, and J. Fontcuberta, Surface symmetry-breaking and strain effects on orbital occupancy in transition metal perovskite epitaxial films, *Nature Communications* 3, 1189 (2012).
- [44] A. Tamai, M. Zingl, E. Rozbicki, E. Cappelli, S. Ricc, A. de la Torre, S. McKeown Walker, F. Y. Bruno, P. D. C. King, W. Meevasana, M. Shi, M. Radovi, N. C. Plumb, A. S. Gibbs, A. P. Mackenzie, C. Berthod, H. U. R. Strand, M. Kim, A. Georges, and F. Baumberger, High-resolution photoemission on Sr_2RuO_4 reveals correlation-enhanced effective spin-orbit coupling and dominantly local self-energies, *Physical Review X* 9, 021048 (2019).
- [45] K. Yamaura, D. P. Young, and E. Takayama-Muromachi, Ferromagnetic transition in the correlated 4d perovskites $\text{SrRu}_{1-x}\text{Rh}_x\text{O}_3$, *Physical Review B* 69, 024410 (2004).
- [46] L. Vaugier, H. Jiang, and S. Biermann, Hubbard U and Hund exchange J in transition metal oxides: Screening versus localization trends from constrained random phase approximation, *Physical Review B* 86, 165105 (2012).
- [47] X. Deng, K. Haule, and G. Kotliar, Transport properties of metallic ruthenates: A DFT+ DMFT investigation, *Physical Review Letters* 116, 256401 (2016).
- [48] Z. Fang, N. Nagaosa, and K. Terakura, Orbital-dependent phase control in $\text{Ca}_{2-x}\text{Sr}_x\text{RuO}_4$ ($0 \leq x \leq 0.5$), *Physical Review B* 69, 045116 (2004).
- [49] B. J. Kim, H. Jin, S. J. Moon, J. Y. Kim, B. G. Park, C. S. Leem, J. Yu, T. W. Noh, C. Kim, S.J. Oh, J.H. Park, V. Durairaj, G. Cao, and E. Rotenberg, Novel $J_{\text{eff}}=1/2$ Mott state induced by relativistic spin-orbit coupling in Sr_2IrO_4 , *Physical Review Letters* 101, 076402 (2008).
- [50] S. J. Moon, H. Jin, K. W. Kim, W. S. Choi, Y. S. Lee, J. Yu, G. Cao, A. Sumi, H. Funakubo, C. Bernhard, and T. W. Noh, Dimensionality-controlled insulator-metal transition and correlated metallic state in 5d transition metal oxides $\text{Sr}_{n+1}\text{Ir}_n\text{O}_{3n+1}$ ($n=1, 2, \text{ and } \infty$), *Physical Review Letters* 101, 226402, (2008).
- [51] G. Zhang and E. Pavarini, Mott transition, spin-orbit effects, and magnetism in Ca_2RuO_4 , *Physical Review B* 95, 075145 (2017).
- [52] G. Van der Laan and B. T. Thole, Local probe for spin-orbit interaction, *Physical Review Letters* 60, 1977 (1988).
- [53] M. A. Laguna-Marco, D. Haskel, N. Souza-Neto, J. C. Lang, V. V. Krishnamurthy, S. Chikara, G. Cao, and M. van Veenendaal, Orbital magnetism and spin-orbit effects in the electronic structure of BaRuO_3 , *Physical Review Letters* 105, 216407 (2010).
- [54] J. P. Clancy, N. Chen, C. Y. Kim, W. F. Chen, K. W. Plumb, B. C. Jeon, T. W. Noh, and Y. J. Kim, Spin-orbit coupling in iridium-based 5d compounds probed by x-ray absorption spectroscopy, *Physical Review B* 86, 195131 (2012).
- [55] J. W. Kim, Y. Choi, S. H. Chun, D. Haskel, D. Yi, R. Ramesh, J. Liu, and P. J. Ryan, Controlling entangled spin-orbit coupling of 5d states with interfacial heterostructure engineering, *Physical Review B* 97, 094426 (2018).
- [56] S. Raj, D. Hashimoto, H. Matsui, S. Souma, T. Sato, T. Takahashi, D. D. Sarma, P. Mahadevan, and S. Oishi, Angle-resolved photoemission spectroscopy of the insulating Na_xWO_3 : Anderson localization, polaron formation, and remnant Fermi surface, *Physical Review Letters* 96, 147603 (2006).
- [57] Z. Zhong, M. Wallerberger, J. M. Tomczak, C. Taranto, N. Parragh, A. Toschi, G. Sangiovanni, and K. Held, Electronics with correlated oxides: $\text{SrVO}_3/\text{SrTiO}_3$ as a Mott transistor, *Physical Review Letters* 114, 246401 (2015).

- [58] E. Pavarini, S. Biermann, A. Poteryaev, A. I. Lichtenstein, A. Georges, and O. K. Andersen, Mott transition and suppression of orbital fluctuations in orthorhombic $3d^1$ perovskites, *Physical Review Letters* 92, 176403 (2004).
- [59] R. Ang, Y. Tanaka, E. Ieki, K. Nakayama, T. Sato, L. J. Li, W. J. Lu, Y. P. Sun, and T. Takahashi, Real-Space coexistence of the melted Mott state and superconductivity in Fe-substituted $1T$ -TaS₂, *Physical Review Letters* 109, 176403 (2012).
- [60] S. Fuchs, E. Gull, M. Troyer, M. Jarrell, and T. Pruschke, Spectral properties of the three-dimensional Hubbard model, *Physical Review B* 83, 235113 (2011).